

FK-array Response to Four Greenland Glacial Earthquakes from Geopsy Transfer Functions

Mustafa Toker

Yuzuncu Yil University, Faculty of Engineering Geophysics Division, Zeve Campus,
65080, Van, Turkey

(Submitted: May 3, 2019; Accepted: July 23, 2019)

Abstract

Using the German Regional Seismic Network (GRSN), we analyzed the Rayleigh waves of four Greenland, $M_w \sim 5$, glacial earthquakes. We obtained their > 30 s period fk-array simulation parameters using the array transfer-functions procedures incorporated in Gpfsimulator GEOPSY software. This analysis has allowed us to estimate their slowness, azimuth and back-azimuth parameters. Further, it also revealed several unique long period phases. These results have enabled us to put the four events in the context of numerous other Greenland glacial events whose source mechanisms do not match those typical of tectonic earthquakes. Instead, they add to the evolving understanding of a new class of source models associated with rapid moving outlet glaciers. Our discussion also includes a summary of the technical details of our analysis and a list of the simulation parameters for the GRSN.

Keywords: Greenland, Glacial earthquakes, Rayleigh waves, FK-array response simulation parameters, Array transfer functions

1 Introduction

The largest glacial earthquakes in Greenland generate longer than 30 s long-period seismograms. They are also similar in magnitude to $M_w = 5$ tectonic earthquakes (*Nettles and Ekström, 2010*). Their long-period signals are even seen at teleseismic distances (*Nettles and Ekström, 2010*), (*Ekström et al., 2003*; *Ekström et al., 2006*). The identification of these special types of earthquakes followed the development and application of a new algorithm designed for the analysis of long-period seismic waves (*Nettles and Ekström, 2010*; *Ekström et al., 2006*). Their distinct characteristics have motivated the development of a new class of earthquake source models.

The new algorithm is based on “array-processing techniques”. Vertical-component seismograms from the global network of seismic stations are filtered between 35 and 150 s. These are then phase adjusted for Rayleigh wave propagation delays from test locations to each station (*Nettles and Ekström, 2010*; *Ekström et al., 2003*; *Ekström et al., 2006*; *Tsai and Ekström, 2007*). When all the signals are in phase the location of the actual epicenter is found. In our case this means the alignment of the corrected Rayleigh wave arrivals for the Greenland events studied here (*Nettles and Ekström, 2010*; *Ekström et al., 2003*).

The initial application of the detection algorithm to Global Seismic Network (GSN) data from 1999–2001 led to the identification of 46 previously unreported $4.6 \leq M \leq 5.0$ events in the glaciated areas of Greenland, Alaska, and Antarctica. Of these, 42 located along the eastern and western coasts of Greenland (*Nettles and Ekström, 2010; Ekström et al., 2003; Ekström et al., 2006; Tsai and Ekström, 2007*). Another fifty-nine glacial earthquakes were detected during 2006–2008 (Table 1) (*Nettles and Ekström, 2010; Kawakatsu, 1989; Stammer, 1992*). Western Greenland currently generates large numbers of glacial earthquakes: Eleven or more earthquakes have been detected in each of the five most recent years, compared with an average of 4.5 events per year for the same region during the period 1993–2003 (*Nettles and Ekström, 2010*).

The glacial earthquakes are consistent with slow source-rise times and depletion of high-frequencies (*Ekström et al., 2003*). These earthquakes generate surface waves that were not well explained by the standard moment-tensor representation of stress release used for tectonic earthquakes. The surface waves were found instead to be well fit by a single-force source model (*Ekström, 2006; Kawakatsu, 1989*), which describes the forces acting on the solid earth during a landslide. This characteristic can be seen in the source parameters of the fifty-nine 2006–2008 events listed in Table 1.

The current study is an extended, complementary version of the previously published research under the title of “the array analyzing of the high quality glacial seismic events active in Greenland using long-period surface (Rayleigh) wave detection by the German Regional Seismic Network (GRSN)” (see *Toker, 2018*). In this study, as different from the previous one, we first review the discovery of glacial earthquakes as a seismological phenomenon. We then discuss the evolving understanding of glacial earthquakes and their association with rapidly moving outlet glaciers in Greenland. We summarize the basic process of the array response simulation procedure for their analysis (*Toker, 2018*). We also analyze and discuss the surface wave characteristics of four Mw~5 Greenland glacial events (*Nettles and Ekström, 2010*). These four glacial events with the magnitudes of $M = 4.9$, 2007-07-04; $M = 4.8$, 2007-07-09; $M = 4.7$, 2007-07-09; and $M = 4.7$, 2007-07-20 are given in Table 1 to update the detection results (see *Toker, 2018* for details). Finally, we list the array response simulation parameters of the four events and their array response images for the GRSN seismic network (GERMAN- GR and GEOFON-GE) (Fig. 1). Our study brings the investigation of Greenland glacial earthquakes updated to 2008.

Table 1. Source parameters for 59 glacial events in Greenland^a (data from *Nettles and Ekström, 2010; Tsai and Ekström, 2007*) and high-quality (A/B) glacial events selected for this study contained in the red bold font.

Date	Time	Latitude	Longitude	<i>M</i>	Date	Time	Latitude	Longitude	<i>M</i>
2006/02/13	20:29:52	70.25	-30.75	4.8C	2007/08/03	19:25:12	72.25	-52.25	4.8C
2006/02/28	22:44:32	69.00	-33.00	4.8A	2007/08/13	20:37:52	66.25	-38.75	4.8B
2006/03/04	23:05:20	65.75	-41.25	4.7B	2007/08/25	09:19:04	75.25	-56.75	4.9A
2006/04/29	11:39:12	65.25	-41.25	4.8B	2007/09/11	22:42:00	70.25	-50.75	4.6C
2006/05/01	06:44:32	72.25	-52.75	4.9A	2007/10/13	05:55:12	74.75	-56.75	4.8A
2006/06/24	10:48:32	69.25	-49.75	4.7E	2007/11/21	18:04:56	66.25	-38.75	5.0A
2006/07/10	18:13:36	65.25	-40.75	4.8A	2007/11/24	00:08:56	68.50	-33.50	4.8A
2006/07/16	03:15:28	69.00	-31.00	4.6C	2007/11/24	12:54:32	66.50	-38.50	4.9A
2006/07/16	06:41:52	73.25	-53.25	4.7C	2007/11/24	13:29:52	67.25	-38.25	4.8A
2006/07/25	04:51:44	68.75	-49.75	4.7C	2007/12/14	06:39:36	75.25	-56.75	4.9A
2006/08/10	18:45:20	77.50	-65.50	4.8B	2007/12/31	14:40:56	66.25	-38.75	4.9A
2006/08/23	17:19:28	65.75	-37.75	4.7C	2008/02/14	05:12:24	72.75	-55.75	4.8B
2006/08/28	07:55:04	69.50	-25.50	4.6B	2008/04/05	21:06:08	75.50	-56.50	4.8A
2006/09/10	04:20:16	77.75	-57.25	4.9C	2008/04/07	13:58:00	74.25	-56.75	4.7C
2006/10/09	04:03:12	76.50	-60.50	4.8B	2008/05/04	12:52:40	65.50	-41.50	4.8B
2006/10/14	07:23:20	76.00	-58.00	4.8B	2008/05/28	21:06:40	70.75	-49.25	4.7B
2006/11/05	09:13:04	75.75	-58.25	4.7C	2008/06/12	17:20:08	69.00	-49.00	4.7E
2006/11/28	10:55:44	68.75	-32.75	4.9B	2008/06/13	15:40:40	75.75	-57.75	4.8C
2006/12/19	16:57:44	74.75	-57.75	4.8B	2008/06/19	15:20:00	74.75	-58.25	4.8B
2007/04/22	08:55:04	66.25	-38.25	4.7A	2008/07/13	04:59:44	69.50	-49.50	4.8C
2007/04/23	21:56:56	75.25	-58.25	4.8A	2008/08/01	14:43:20	66.50	-38.50	4.8A
2007/05/30	02:57:12	77.50	-63.50	4.7C	2008/08/01	23:00:40	66.75	-39.25	4.8A
2007/06/09	05:16:56	75.75	-60.75	4.8B	2008/08/14	20:58:24	77.75	-58.75	5.0A
2007/07/04	16:55:20	69.25	-49.75	4.9A	2008/08/19	21:05:28	66.25	-38.25	4.8B
2007/07/09	01:08:16	66.25	-37.25	4.8A	2008/11/03	16:44:48	68.75	-33.75	4.9B
2007/07/09	02:42:08	66.75	-38.25	4.7B	2008/11/07	13:44:24	77.50	-66.50	4.7E
2007/07/09	05:31:12	75.00	-57.00	4.6C	2008/11/21	20:31:52	76.00	-58.00	4.9A
2007/07/20	00:36:16	69.25	-33.25	4.7A	2008/11/25	04:10:40	68.50	-33.50	4.9A
2007/07/24	23:03:12	77.25	-60.75	4.9A	2008/12/13	14:47:52	68.00	-34.00	5.0A
2007/07/26	22:42:48	66.50	-38.50	4.7A					

^aOrigin times and epicenters for 59 glacial earthquakes in Greenland, 2006–2008. The letter code following the magnitude *M* indicates the quality of the detection and location: A/B is the highest quality and C/E is the lowest.

2 Greenland glacial seismicity

The glacial seismicity describes a new class of seismic events. These events occur in Polar Regions with moving outlet glaciers in Greenland, Alaska and Antarctica (*Nettles and Ekström, 2010; Ekström et al., 2003*). In this section, we briefly review the current understanding of glacial earthquakes, their detection and association with rapidly moving outlet glaciers in Greenland.

Glacial seismic events produce large-amplitude and long-period seismic waves. Conventional techniques of seismic monitoring are not be used to detect them, due to the technical differences in signal detection process. Their existence was therefore not known until 2003, when the application of a new method of earthquake detection revealed the occurrence of dozens of earthquakes with distinct characteristics in glaciated areas of Greenland, Antarctica, and Alaska (*Nettles and Ekström, 2010; Ekström et al., 2003; Tsai and Ekström, 2007*). Glacial seismicity represents one of several phenomena related to rapid changes in the dynamics of glaciers that have received increasing atten-

tion in the context of changing climate conditions (e.g., global warming). The distributional pattern of glacial seismicity was found to be a seasonal phenomenon. This pattern was spatially correlated with major outlet glaciers of the Greenland ice sheet and tightly clustered near a number of Greenland's large outlet glaciers (e.g., typical source durations were ~ 50 s and mass transport was in the range of 0.1 to 2.0×10^{14} kg m) (*Nettles and Ekström, 2010; Ekström et al., 2003; Tsai and Ekström, 2007*).

The glacial seismic events are considered to be associated with large scale calving events as the main seismogenic source; the collapse of a large ice mass into the glacial fjord generates a small tsunami and the tsunami arrival times constrain the timing of the ice-loss events (*Nettles and Ekström, 2010; Ekström et al., 2003; Tsai and Ekström, 2007*). A striking feature of the glacial event distribution indicates that all events occur in association with large tidewater glaciers and calving events. The overall event distribution is abundant where marine-terminating outlet glaciers are observed, consistent with the marine-calving source mechanism (*Nettles and Ekström, 2010*). However, glacial seismicity is not observed in and around the places where the highest concentration of land terminating glaciers is found (e.g., *Moon and Joughin, 2008*), and where many glaciers drain into floating ice shelves. Seasonal advance (winter) and retreat (summer) of the outlet glaciers are achieved by the reduction and/or shutdown in large-scale calving during the winter, with an increase in calving during the summer. The link between large-scale calving events and glacial earthquakes then explains the seasonal signal in earthquake occurrence at glaciers (*Nettles and Ekström, 2010; Ekström et al., 2003; Tsai and Ekström, 2007; Moon and Joughin, 2008*).

The cross-flow width and the thickness of the glacier are the most important parameters which describe and limit the maximum magnitude of an earthquake at a given glacier near its terminus, and combine to produce a characteristic range of earthquake magnitudes at each glacier (*Nettles and Ekström, 2010; Ekström et al., 2003; Tsai and Ekström, 2007*). The glacier exhibits no coseismic displacement, but rather an increase in the amplitude of the velocity which is largest near the calving front. Since the thickness controls both along-flow width and the sliding distance, suggesting that the glacier thickness provides the strongest control on the observed event magnitudes (*Nettles and Ekström, 2010*).

3 *GRSN array and data processing*

Throughout our study, we processed data obtained from GRSN consisting of the large regional GERMAN (GR) and GEOFON (GE) arrays (<http://geofon.gfz-potsdam.de/waveform/archive/index.php>) (see *Toker, 2018*). Fig. 1a shows the configuration of the GRSN array and the layout of the seismometer sites for the regional arrays. GRSN (Fig. 1a) (*Korn, 2002*) comprises 16 STS2 digital broadband stations with a flat, velocity-proportional response characteristic in the frequency range of 8.33 mHz to 40 Hz (*Trnkoczy et al., 2009*). GRSN is designed to monitor and collect high-quality data from regional and global seismic events as well as recording and locating all events with $M_l > 2$ in German territory. All stations are continuously recorded and, with one excep-

tion, are connected via the Internet with each other and with the network center at the Gräfenberg Observatory (GRFO) in Erlangen (*Trnkoczy et al.*, 2009) (Fig. 1a). GRSN is a combination of a physical and a virtual network (for more details, see <http://www.szgrf.bgr.de/>).

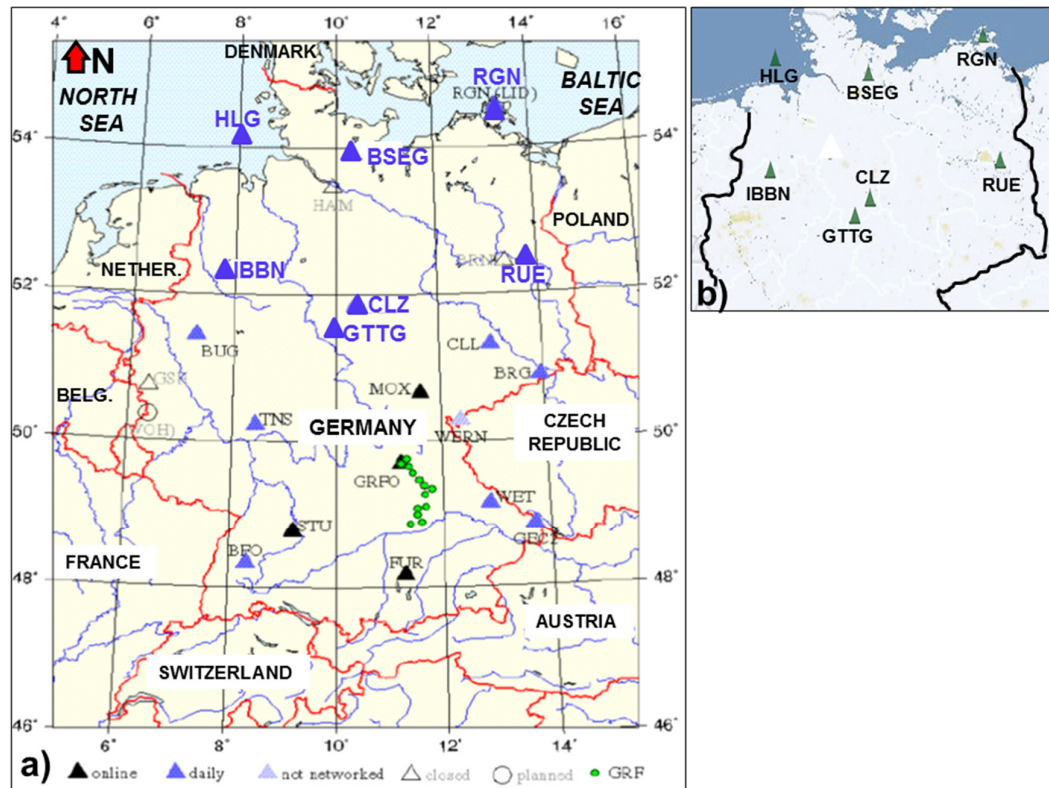


Fig. 1. **a.** Map of the station sites of GRSN (site details are given in the legend) shows the locations of the stations (large blue fonts and triangles; HLG, BSEG, RGN, IBBN, CLZ, GTTG, RUE) used in our analyses (map reproduced from *Trnkoczy et al.*, 2009). **b.** The inset map shows the simple array geometry of these seven stations used in this study with the reference stations assigned; GTTG and CLZ (see text for details) (*Toker*, 2018).

In this study, the GRSN array was defined by a set of stations; RUE, GTTG, CLZ, RGN, IBBN, BSEG, and HLG with two stations, CLZ and GTTG, being assigned the role of reference sites (Fig. 1a). The relative distances from these reference points to all other array sites are used later in all array specific analysis algorithms. As the four glacial events (Table 1) were recorded only at the seven stations; RUE, GTTG, CLZ, RGN, IBBN, BSEG, and HLG (Fig. 1b), these stations form the array geometry used in this study, providing suitable station configuration with an adequate data set for our analyses. The recorded events from Germany were processed with Seismic Handler Motif (SHM) improved by K. Stammler (*Stammler*, 1992), which is used for waveform retrieval and data analysis (*Trnkoczy et al.*, 2009) (*Bormann* (2012)). Seismic arrays are generally different from local seismic networks mainly by the methods used for signal analysis being superior to three-component stations in terms of improving the quality of seismic stations and detecting and characterizing signals from earthquakes (*Trnkoczy et*

al., 2009; *Schweitzer et al.*, 2009). Array processing technique used in this study requires high-level signal coherency across the array. This places important constraints on the array geometry, spatial extent, and data quality (*Schweitzer et al.*, 2009). The appropriate analysis of the array data depends on a stable, high-precision relative timing of all the array elements and small temporal differences in the arrival of seismic signals between the different sensors play an important role in all array-processing techniques (*Schweitzer et al.*, 2009). Hence, the signal detection capabilities of arrays are obtained by applying the beamforming technique, which suppresses noise while preserving the signal, thus enhancing the signal-to-noise ratio (SNR). In addition, array parameters, the station-to-event azimuth (backazimuth) and the apparent velocity (slowness) of various styles of event signals, are also estimated from arrays. These parameters are essential for both event relocation and the classification of signals (*Schweitzer et al.*, 2009).

In this study, the general seismic array processing beamforming technique was applied using SHM to analyze the event signals. SHM used in this study is an interactive analysis program preferably used with continuous waveform data (*Stammler*, 1992). It was developed at the Seismological Observatory Gräfenberg and in this study was used in the routine analysis of the four detected glacial events (*Trnkoczy et al.*, 2009) (Table 1 and Fig. 1). SHM is well suited to the analysis of glacial seismic data since it has advanced features for trace manipulations and automatic or semiautomatic phase picks (see *Stammler*, 1992 for details). The basic tools and features of SHM are built around reading traces of the detected events from continuous data streams in Stein-compressed MiniSEED files associated with a set of standard filters (simulation filters and Butterworth filters) on broadband input traces of the events (see also *Stammler*, 1992). Teleseismic beam traces using array-beamforming are computed using SHM. The slowness and back-azimuth of an incoming wavefront for array processing are also determined. The detected events are located using the LOCSAT program. Moreover, in this paper, the applied procedures for estimating the slowness parameter, the angles of approach (azimuth-backazimuth) of detected event signals and processing algorithms for event detection are briefly described. This study also documents array-processing technique with concluding remarks from the SHM for detecting and associates event signals from regional seismic events using the array installation data from the regional GERMAN (GR) and GEOFON (GE).

The automatic processing steps in SHM are divided into three separate cases (*Toker*, 2018): a) Event array processing to associate phase arrivals to define events, b) event signal detection using beamforming, filtering, and location-relocation, and c) signal attribute to estimate the array parameters; slowness, azimuth and/or back-azimuth. Finally, we compute array transfer functions for fk -array response to four glacial earthquakes (Table 1) from Geopsy transfer functions (Gpfxsimulator, GEOPSY) and estimate fk -array simulation parameters using the transfer-functions procedures incorporated in Gpfxsimulator GEOPSY software.

4 Results and interpretation

The source parameters of the four glacial events in Greenland are given in Table 1 and were recorded in GRSN stations; HLG, BSEG, IBBN, RGN, CLZ, GTTG, and RUE (Fig. 1b). The recorded glacial events from the GRSN network were processed and seismic array beamforming and alignment of the events were performed by SHM (Toker, 2018). The waveform resemblances (vertical component-Z) and power spectrum of the recorded four events from the seven stations are shown in Figs. 2–5.

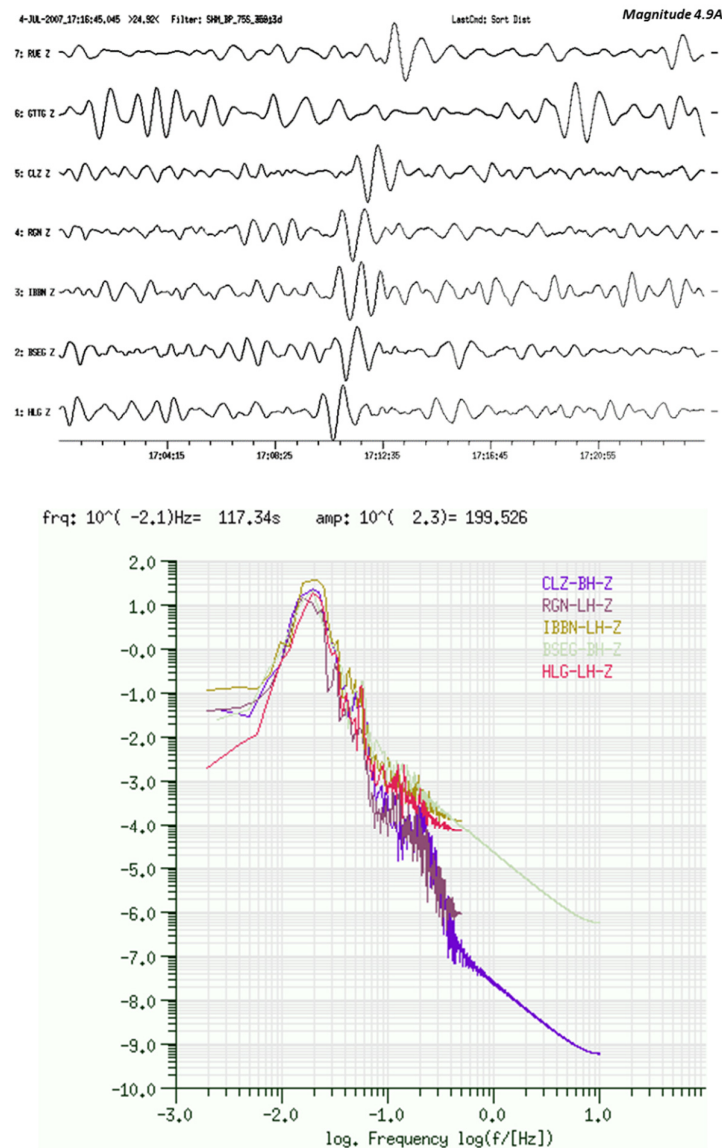


Fig. 2. Mean root square residual: 0.51, distance: 32.5, beam-slowness: 29.0 ± 0.4 (x), beam-azimuth: 322.4 ± 0.5 (x), reference: CLZ, origin time: **4-JUL-2007_16:55:20.000**, epicenter: 69.25 lat. -49.75 lon. and FE region: Western Greenland (Kalaallit Nunaat) (at top). Power spectrum overlap for this event is also performed (fit line) at each station used in this study (at bottom, various colors denote each station).

The waveforms presented in Figs. 2–5 show the surface wave peaks of the detected glacial events observed at the GRSN network, the aligned traces of all single observations associated with their power spectra. Following the same procedures given by (Stammler, 1992), all the signal traces were adjusted and relocated to provide the alignment of the event pulses. The SNR of an observed signal calculated by summing the coherent event signals from the array sites was improved with an array. All the seismic data were filtered with Butterworth band-pass filter between 35s and 70s and are displayed with a common amplification. All the signal traces were aligned and summed without any delay-time application. The important process during the beamforming was to identify the delay times, with which the single signal traces were shifted before summation ('delay and sum') to obtain the highest amplitude due to the coherent interference of the observed event signals (Stammler, 1992). The onset times of the event signal on each trace were simply picked and the traces were shifted with respect to the onset time at the reference site of the array. Based on the same data set and GRSN array reported by Toker, (2018), further analyses associated with the computational process and technical details are given in the following subsections.

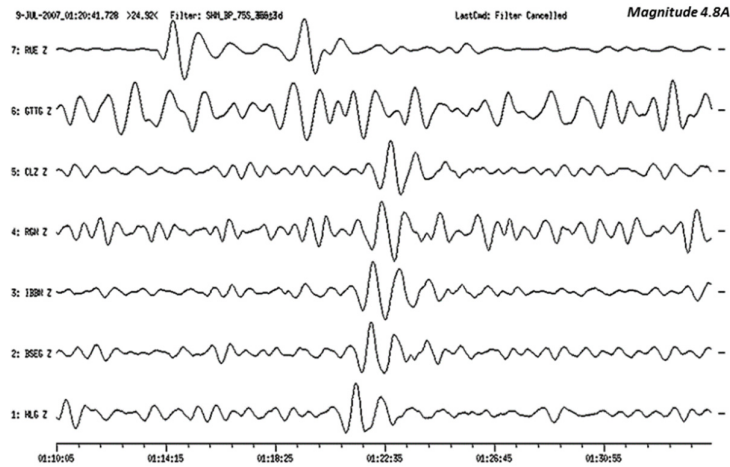


Fig. 3. Mean root square residual: 0.70, distance: 27.6, beam-slowness: 28.9 ± 0.7 (x), beam-azimuth: 314.5 ± 1.2 (x), reference: GTTG, origin time: **9-JUL-2007_01:08:16.000**, epicenter: 66.25 lat. -37.25 lon. and FE region: Eastern Greenland (Kalaallit Nunaat).

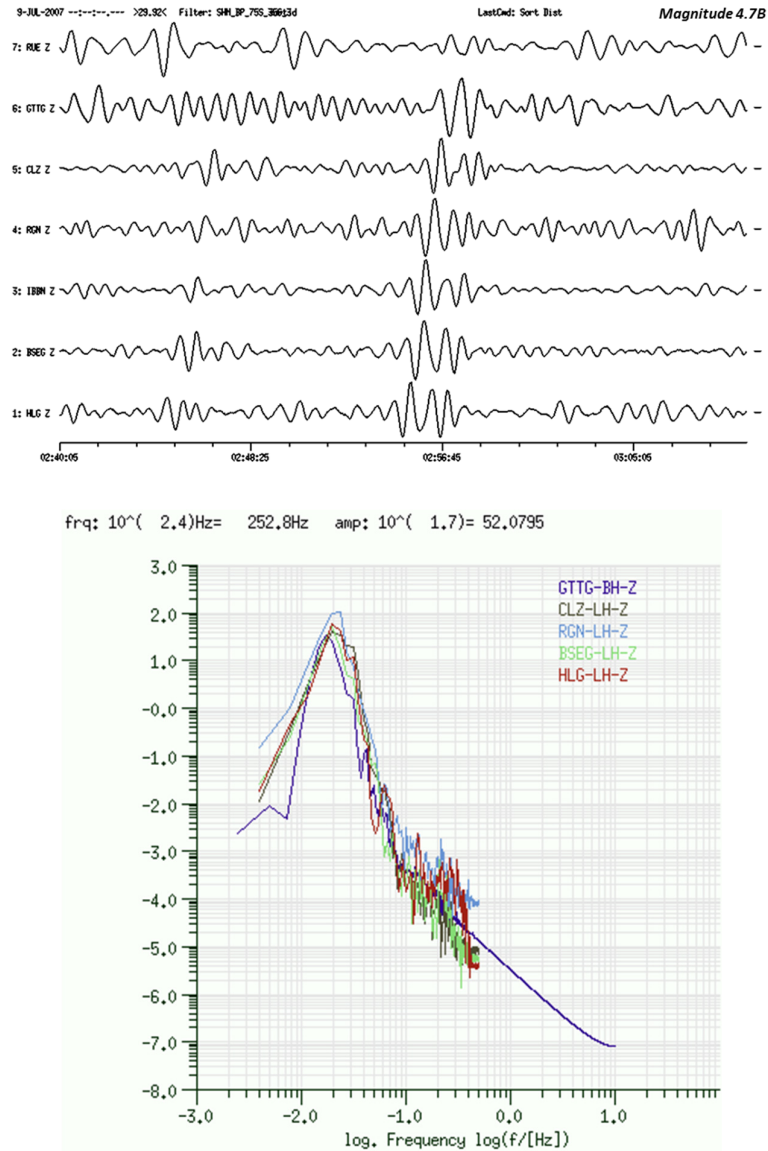


Fig. 4. Mean root square residual: 0.83, distance: 28.1, beam-slowness: 29.6 ± 0.9 (x), beam-azimuth: 312.4 ± 1.4 (x), reference: CLZ, origin time: **9-JUL-2007_02:42:08.000**, epicenter: 66.75 lat. -38.25 lon. and FE region: Eastern Greenland (Kalaallit Nunaat) (at top). Power spectrum overlap for this event is also performed (fit line) at each station used in this study (at bottom, various colors denote each station) (the same as the event shown in Fig. 3).

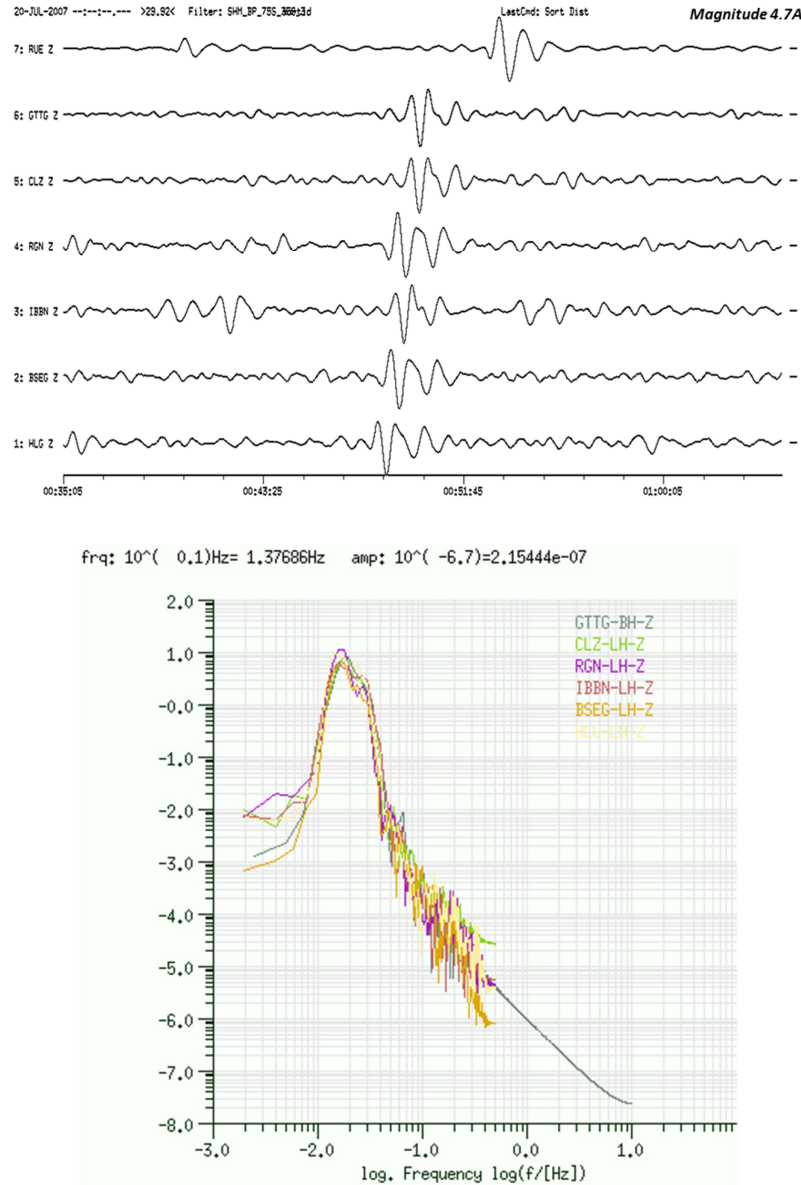


Fig. 5. Mean root square residual: 1.38, distance: 26.8, beam-slowness: 30.0 ± 0.8 (x), beam-azimuth: 323.3 ± 1.2 (x), reference: CLZ, origin time: **20-JUL-2007_00:36:16.000**, epicenter: 69.25 lat. -33.25 lon. and FE region: Eastern Greenland (Kalaallit Nunaat) (at top). Power spectrum overlap for this event is also performed (fit line) at each station used in this study (at bottom, various colors denote each station).

4.1 Computation

Initially, the seismic data from the GRSN network are installed and read in the appropriate data window of SHM for monitoring and analyzing the event signals. The Butterworth bandpass filter is chosen to provide a good SNR. The slowness and azimuth of incoming waves are determined using visible minimum / maximum peaks of automatically picked up signals; then, the Plane Wave option of SHM is called. The resulting slowness and azimuth were checked using the Beam option of SHM to correct some of the essential phase readings and then, Location is called and the event is locat-

ed. The following subsections present the stages of how the installed seismic data is read, monitored and analyzed using SHM software (see Stammler, 1992 for details).

Reading the MiniSEED data format; the MiniSEED data format used in this study is a subformat of the commonly used SEED data format. It is suited to continuous data or for storing long time spans of data (Stammler, 1992). SHM accesses the MiniSEED format by start time and read length and reads only part of the file rather than reading a filename completely. SEED and MiniSEED data formats are quite flexible and allow a large variety of subformat types. For reading the MiniSEED data with the read option, the dialog box of SHM should be correctly configured.

MiniSEED files are prepared as the GRSN stations are inserted (Fig. 1a). When all the stations have been configured, the menu entry Read is selected. This opens a dialog box. The appropriate buttons for stations, data channel (e.g., BH, LH, and HH) and component(s) (east-west, north-south, and z-vertical component) are selected. Date and time are chosen using the arrow buttons above and below the time field. The data are entered by specifying the station list, channel code, start time, read length, and components as shown in Figs. 2–5. In order to find the data file(s) to be read, SHM needs to have a directory file which contains the information about the location, filename and content of MiniSEED files called *sfdfile.sfd* (*sfd* refers to seed file directory) and resides in the data directory. SHM reads data that are given in such a file. Before processing the data in the MiniSEED format, *sfdfile* requires to be updated. The SHM package also contains a program to create *sfdfile.sfd*. After *sfdfile.sfd* has been generated, SHM reads the data files given. The SHM command for reading the MiniSEED data needs to have the location of the *sfdfile.sfd*.

Reading and filtering data; the requested data streams and time window are selected by opening a dialog box of the menu entry Read (the interface to the MiniSEED formatted data). The essential parameters; station list, channel, component, start time, length of time window and location of the directory file (*sfdfile.sfd*.) are chosen. Then, the Filter menu entry is selected and the desired Bandpass filter (35s-70s) is chosen in broadband waveform data. The filter is applied to the traces on the display and the read-in traces are filtered automatically. Then, the filtering is carried out on all the traces of the display if no trace has been previously selected. The resulting traces are displayed on the screen.

Plane wave; the epicentral distances of the recorded glacial events are larger than the aperture of the recording array of GRSN (Fig. 1). The major frequencies of the picked signals are in a range in which signal coherency is possible, indicating waveform similarity on the recording array (Figs. 2–5). Hence, the plane wave algorithm of SHM is applicable. Considering that the wavefront of the phase is a plane wave, the menu entry Plane Wave of SHM computes the array parameters, the slowness and backazimuth from coherent phases and uses all the phases of the name provided in the phase dialog box (Figs. 2–5). This algorithm detects the best fitting of the wave plane and parameterizes it by back-azimuth and slowness. The concluding values are given in the analysis parameter box and checked with the command Beam. The entry Beam needs to have the location entries (Lat. and Lon.) of the recording stations in the station information file.

Locating and sorting distances; after the locations (Lat. and Lon.) of the events have been manually written in the analysis parameter box and the appropriate settings of the reference stations have been checked, the epicentral distances to the chosen reference stations and the corresponding slowness are computed using the correction for ellipticity of the earth and the results entered into the analysis parameter box are shown. As a result, the epicenter locations are determined and all the traces are sorted according to the epicentral distance.

4.2 Parameterization

The GRSN array geometry (Fig. 1b) is defined by seismometers with two seismometers being assigned the roles of the two reference sites (CLZ, GTTG) during the data processing. The relative distances from the reference points to all other array sites are used in all array specific analysis algorithms.

A seismic wave approaches a given array with a plane wave front for much larger distances from the source (more than 10 wavelengths) (*Stammler, 1992; Trnkoczy et al., 2009; Schweitzer et al., 2009*). The propagation directions of the plane wave front projected onto the horizontal plane are basically identified by the two main angles; Φ and Θ (*Schweitzer et al., 2009*). Φ is the backazimuth, also called beam-azimuth, which is an angle-of-wavefront approach, measured clockwise between the north and the direction towards the epicenter in $[\circ]$. Θ refers to the direction in which the wavefront propagates is also measured in $[\circ]$ from the north with $\Theta = \Phi \pm 180^\circ$. The angle observed between the direction of approach and the vertical plane is called the angle of incidence i with $i \leq 90^\circ$. The seismic velocity below the array site and the angle of incidence define the apparent propagation speed of the wavefront crossing the array site.

The crustal velocity with the incidence angle determines the propagation speed of the wavefront at the instruments and is called an apparent velocity v_{app} (not the physical propagation speed). v_{app} is absolute value of the apparent velocity vector in [km/s] of a plane wave crossing an array and a constant for a specific seismic ray traveling through a layered Earth model. Apparent velocity vector \mathbf{v}_{app} is given by $v_{app} = 1 / s \cdot \mathbf{v}_{app} = (v_{app, x}, v_{app, y}, v_{app, z})$, where $(v_{app, x}, v_{app, y}, v_{app, z})$ are the apparent velocity components in [km/s] of the wavefront crossing an array site. The inverse of the apparent velocity is called slowness s (a constant for a specific ray), which we call beam-slowness here. The slowness unit is [s/km] for local or regional studies and [s/ $^\circ$] for global applications (the slowness is also known as the ray parameter). s slowness vector is given by $\mathbf{s} = 1 / v_{app} \cdot \mathbf{s} = (s_x, s_y, s_z)$, where (s_x, s_y, s_z) are the inverse apparent velocity (= slowness) components in [s/km].

The computed array parameters of the events are given in Table 2 and their locations are shown in Fig. 6 (reproduced from *Toker, 2018*).

Table 2. Summary of the array parameters of the detected events (see Table 1 for the source mechanisms of the selected events and Fig. 1 for reference stations).

Glacial events	RMS	Dist.	beam-slow-ness	beam-az-imuth	epi-slow-ness epi-azimuth	Depth	Ref.	Origin time	Epi. Lat. - Lon.	FE region
<i>Event 1</i>	0.70	27.6	28.9± 0.7 (x)	314.5± 1.2 (x)	not specified	0.0	GTTG	9-JUL-2007_01:08:16.000	66.25 37.25	Eastern Kalaallit Nunaat
<i>Event 2</i>	0.83	28.1	29.6± 0.9 (x)	312.4± 1.4 (x)	not specified	0.0	CLZ	9-JUL-2007_02:42:08.000	66.75 38.25	Eastern Kalaallit Nunaat
<i>Event 3</i>	1.38	26.8	30.0± 0.8 (x)	323.3± 1.2 (x)	not specified	0.0	CLZ	20-JUL-2007_00:36:16.000	69.25 33.25	Eastern Kalaallit Nunaat
<i>Event 4</i>	0.51	32.5	29.0± 0.4 (x)	322.4± 0.5 (x)	not specified	0.0	CLZ	4-JUL-2007_16:55:20.000	69.25 49.75	Western Kalaallit Nunaat

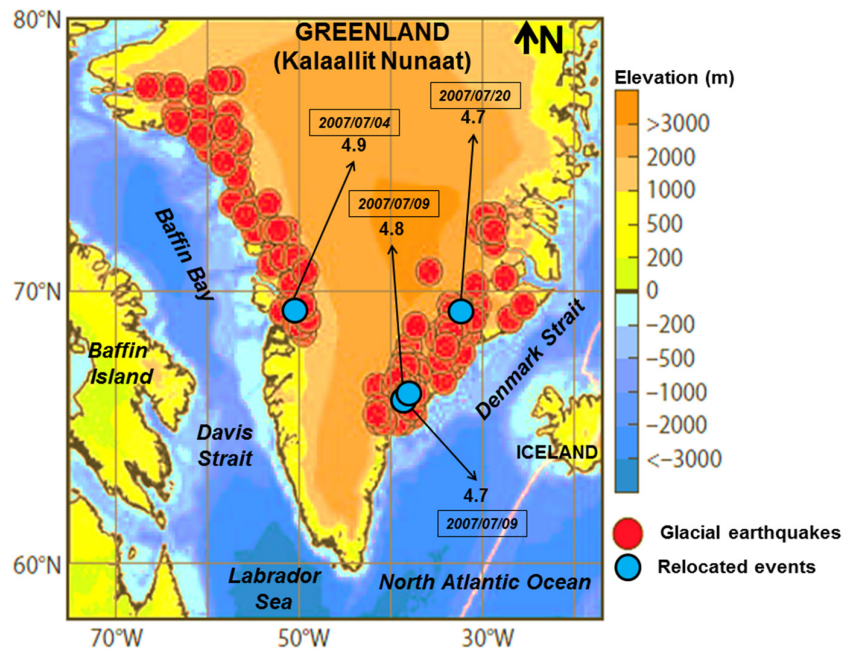


Fig. 6. Glacial seismicity map showing 252 glacial earthquakes in Greenland for the period 1993–2008, detected and located using the surface-wave detection algorithm (data from *Nettles and Ekström, 2010*) and analyzed in detail by *Tsai and Ekström, (2007)* (map modified and adapted from *Nettles and Ekström, 2010*) and also the locations of the four glacial events (magnitude and time) selected and analyzed in this study (see Tables 1 and 2 for related parameters in *Toker, 2018*). The tight clustering of the relocated epicenters is obvious near major outlet glaciers (*Nettles and Ekström, 2010; Moon and Joughin, 2008*).

4.3 *FK-Array response*

The event signals in the glacial data collected from the GRSN network are detected during the data processing by SHM in this study. The signals of plane waves recorded at different sites of the GRSN array are more coherent than random noise. These signals are considered to be very distinct from the background noise due to their amplitudes, magnitudes, different shapes, and/or frequency contents (Figs. 2–5 and Table 2). The delay times for each detected event at each station are automatically defined to calculate an array beam as shown in Figs. 2–5 by a specific beam-azimuth and beam-slowness combination. The calculated delay times and array beams are dependent on the position of the single sites with respect to the reference points (CLZ and GTTG) of the GRSN array (Fig. 1b) and to the backazimuth of the signal. The noises and amplitude differences in the signals influence the beam quality and hence, the improvement of the SNR due to the beamforming is essential (*Trnkoczy et al., 2009; Schweitzer et al., 2009*). The event signals shown in Figs. 2–5 indicate forming signals with beam-slowness and comparing the amplitudes of the beams and reveal the best slowness-backazimuth combination that provides the maximum energy on the beam and various array responses that can be produced by array transfer functions (*Schweitzer et al., 2009*). The filtering-beamforming and beamforming-filtering processes are also performed to test the traces and beams, although both procedures give the same result.

In this study, we also compute array transfer functions for fk-array response to four glacial earthquakes (Table 1) from Geopsy transfer functions (Gpfsimulator, GEOPSY). The relative coordinates “x” and “y”, azimuth and slowness are provided by SHM parameter information for each detected glacial event (Table 2). The resulting slowness and azimuths are checked using the Beam option of SHM. The delay times for each station by a specific backazimuth and apparent velocity combination are defined to calculate an array beam. The calculated delay times depend on the relative position of the single sites with respect to the array’s reference point and to the backazimuth of the seismic signal. GRSN stations used for fk-array response simulation are given in Fig. 7. The estimated simulation parameters for array responses shown in Figs. 8 and 9 are the following; Bandpass filter: 35s-70s; Frequency (f) range: 0.02857-0.01429 *Hz*; The best frequency value to use for response image: 0.02 *Hz* (decimals not changed: the values 0.03 and 0.01 are out of the range); Velocity: 1700 m/s (for Plio-Quaternary sediments) and the corresponding wavenumber (k) range: 0.0001056-5.2816e-5.

FK-array transfer function is interpreted to describe sensitivity and resolution of GRSN array (Fig. 7) for glacial seismic signals with different frequency contents and slownesses (Figs. 8 and 9). It produces various array responses (i.e., when digitizing the output from a seismometer, we sample the wavefront of a seismic signal in the time domain and/or, when observing a seismic signal using an array, we obtain a spatial sampling of the ground movement) (*Schweitzer et al., 2009*). Hence, with GRSN array, we estimate the wavenumber k of the wave defined by its wavelength λ (or frequency f) and its slowness s , suggesting that the transfer function of GRSN array is not only dependent on the slowness of the glacial seismic phase observed with this array, but is also

a function of the wavenumber k (i.e., wavelength or frequency) of the observed glacial signal, and of GRSN array geometry (Fig. 7).

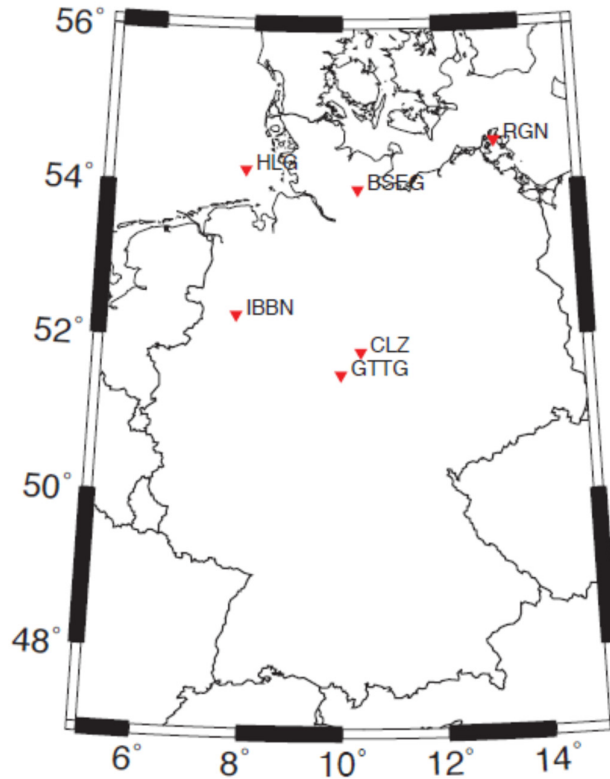


Fig. 7. GRSN stations used for FK Array response simulation.

The aperture and geometry of GRSN array define the resolution of the array for small wavenumbers and the azimuth dependence, respectively (Figs. 8 and 9). The larger the aperture is, the smaller the wavenumbers (or slownesses) is that can be measured with the array. For example, the number of sites controls the quality of the array as a wavenumber filter, i.e., its ability to suppress energy crossing the array (*Schweitzer et al.*, 2009). The distances between the seismometers also define the position of the side lobes in the array transfer function and the largest resolvable wavenumber: the smaller the mean distance, the smaller the wavelength of a resolvable seismic phase will be (for a given seismic velocity). In two samples of array transfer functions (Figs. 8 and 9), the GRSN array shows resolution differences in different azimuths (see Table 2), which are caused by its geometry (Fig. 7). The many side lobes of the transfer function are the result of the large distances between the single array sites.

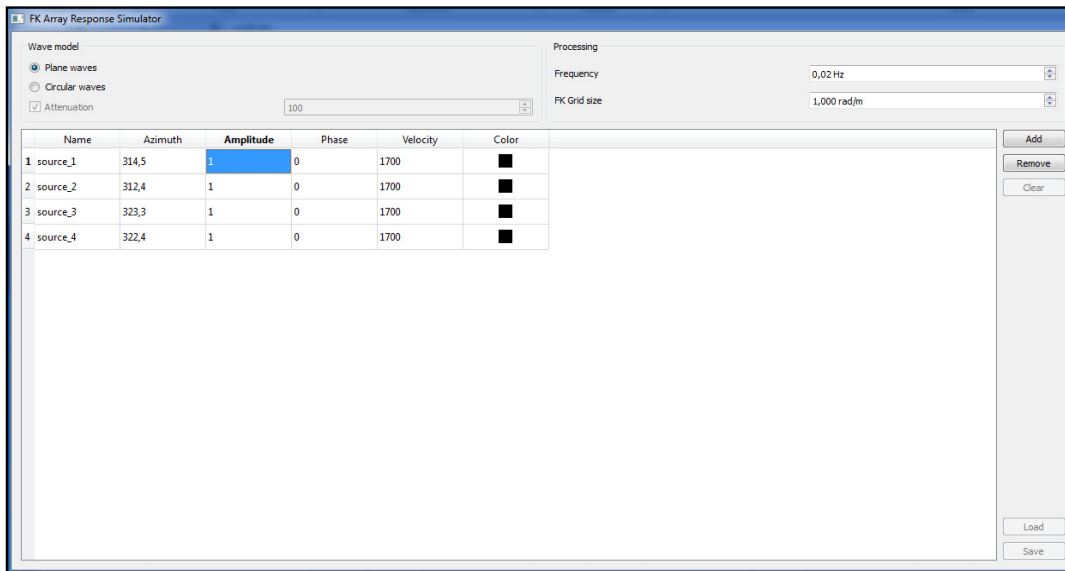
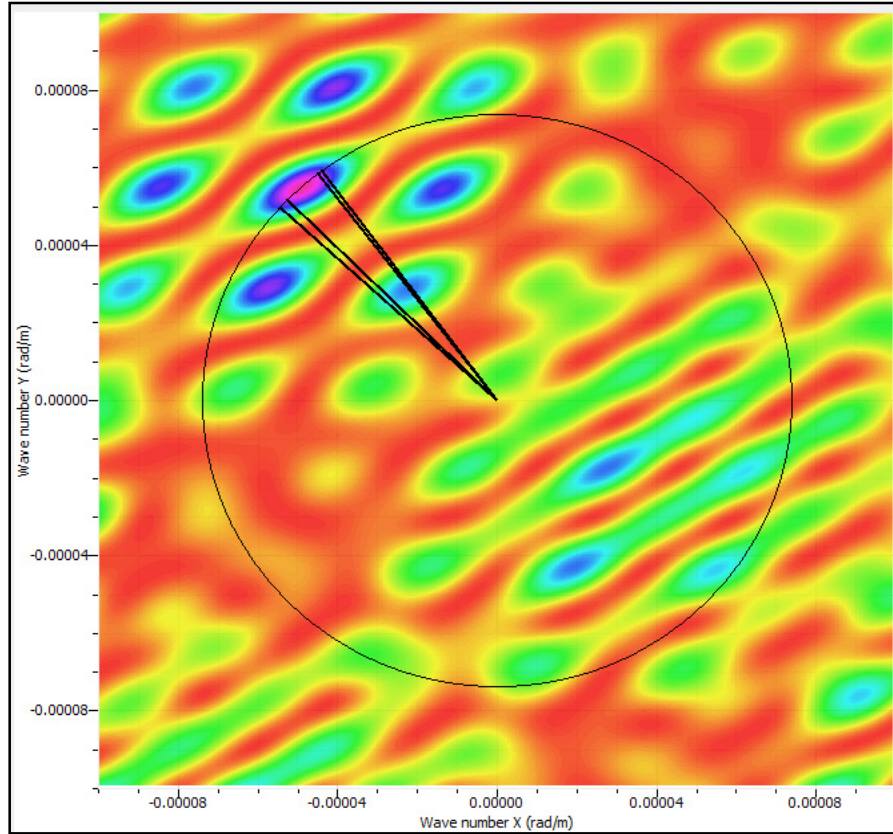


Fig. 8. FK Array response (top) and simulation parameters (bottom) of the four glacial events with their azimuths (see Table 2). Wavenumber (k): 0.0001056 (rad/m), frequency (f): 0.02 Hz, FK Grid size: 1,000 rad/m, velocity: 1700 m/s.

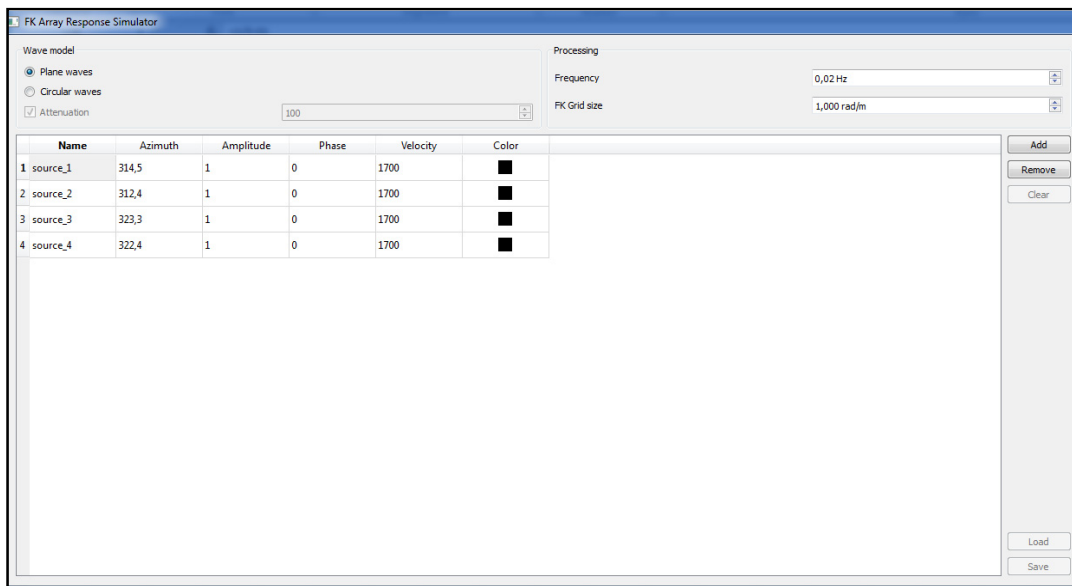
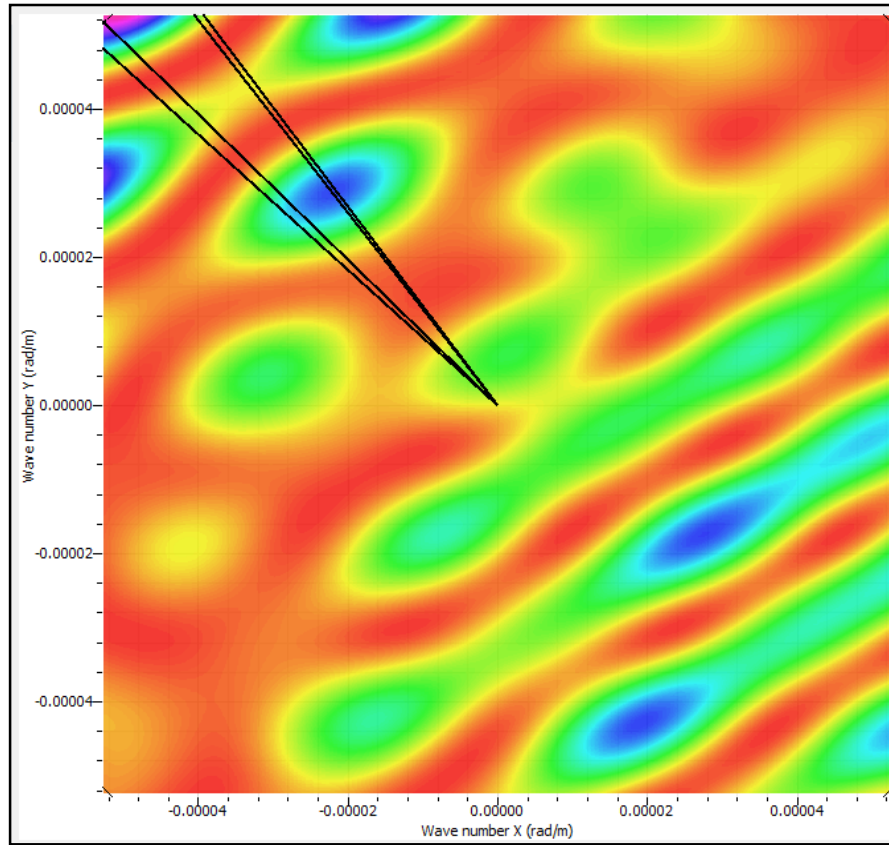


Fig. 9. FK Array response (top) and simulation parameters (bottom) of the four glacial events with their azimuths (see Table 2). Wavenumber (k): 5.2816×10^{-5} (rad/m), frequency (f): 0.02 Hz, FK Grid size: 1,000 rad/m, velocity: 1700 m/s.

5 Discussion

In this study, we estimated FK-array response to four Greenland glacial earthquakes from Geopsy transfer functions. The time delays of the event signals observed at GRSN stations were mainly used for the data processing. For this reason, the small time windows ($\sim 25\text{--}30$ min.) for the analysis of seismic phases were carefully selected. A direct estimate of the beam-azimuth and the beam-slowness of the signals were provided.

Analytical performance of GRSN array was observed from the FK-array response (Capon, 1969). The array response specified the power gain over the horizontal wave-number $k = (k_x, k_y)$ that unveils the sharpness of the main circle, the location and amplitude of small side lobes (Haubrich, 1968). The array response well-arranged certain ray paths and the event locations. Since, the relocation capability of the recorded events (e.g., the sources of the event signals) is related to the resolution quality of the recorded signal in the FK-array response. FK-array analysis also calculated beam-slowness and beam-azimuth from the time lags by performing a grid search over various incident angles, calculating the power distributed among different slownesses and directions of approach (Capon, 1969; Harjes and Henger, 1973), and finding the maximum energy in the stacked time window (see Rost and Thomas, 2003 for other approaches). Beam-azimuth and beam-slowness estimated for each single phase allowed for consistency controls on common azimuths and correct order of phase arrivals observed. As a result, the error limits for the estimated array parameters were easily derived from the size (e.g., width) of the main circle in the array response which resembles the distribution of stations over the aperture of GRSN array (also see Harjes and Henger, 1973) (Fig. 7).

In this study, the elevated SNR of beam traces enabled the detection of glacial events, which are undetectable in single station-type conventional analyses. Hence, it is to say that the GRSN array is relatively well-suited to detect such long-period events. Interestingly, the GRSN array acts as a wave number k -filter (Rost and Thomas, 2003). Since, the beamforming process only works for a correct beam-slowness and beam-azimuth combination, amplifies phases with the appropriate beam-slowness and suppresses incoherent noises. The noise suppression quality depends on the number of stations of the GRSN array to form a beam that we need. For example, a plain summation of the observed traces leads to a high-amplitude waveform in the summation trace. However, incorrect combination of beam-slowness and beam-azimuth can lead to a low-amplitude waveform. In our case, the high-amplitude beam traces and directivity of the incident wave fields made the relocation of events possible with a GRSN array that we used. The GRSN array enhanced event arrivals out of the noise by summing for various slownesses and thus, acted as a velocity filtering of the wave field (Harjes and Henger, 1973; Rost and Thomas, 2003) and finally, allowed the detection of the long-period surface wave phases.

Finally, the FK-array response to four Greenland glacial earthquakes from transfer functions indicated several small lobes with a suppression of the power next to the main circle, which was controlled by the aperture design, number of array stations, configura-

tional pattern, and interstation spacing of the GRSN array. The aperture of the GRSN array controlled the resolution ability of the array in order to separate the wave numbers of the incoming wave fronts. The geometry of the GRSN array affected the azimuthal dependency, the resolution, the quality and the location of the lobes (*Harjes and Henger, 1973; Rost and Thomas, 2003*). The number of stations controlled the suppression of energy crossing the GRSN array with various slowness vectors. The interstation spacing of the GRSN array defined the location of the small lobes and the largest resolvable wave number (e.g., the smaller the interstation spacing, the larger the wavelength of the phase, (*Rost and Thomas, 2003*). In this study, our results conclude that the GRSN array gave an acceptable array transfer function, even though this array was relatively well-suited to detect, at least, long-period surface waves. Since, it showed an azimuthal dependence of the array response function and of the resolution with small lobes close to the main circle (see *Harjes and Henger, 1973* for triangle and rectangle-shaped arrays; *Rost and Thomas, 2003*).

6 Conclusions

In this study, we detected four long-period glacial events; M 4.9, 2007-07-04; M 4.8, 2007-07-09; M 4.7, 2007-07-09; and M 4.7, 2007-07-20 recorded at the stations of the GRSN array (GR and GE) and monitored the waveform patterns of these events for Greenland updated through 2008. The array geometry (GRSN) was defined by a set of seven stations; RUE, GTTG, CLZ, RGN, IBBN, BSEG, and HLG. The stations, CLZ and GTTG, were assigned the role of reference sites. We used the long-period surface waves (Rayleigh) to detect and analyze this new class of earthquake model in the context of array processing technique and array parameters using SHM.

The GRSN array geometry was processed to associate phase arrivals to identify glacial events. The surface wave characteristics of the detected events with magnitudes; M 4.9; M 4.8; M 4.7; and M 4.7, were provided to update the detection results. The glacial event signals were detected for use in the beamforming, filtering, and location-relocation steps. All the seismic data were filtered with Butterworth band-pass filter between 35s and 70s and were displayed with a common amplification. The beam traces using array-beamforming were computed using SHM. The beam-slowness (the apparent velocity) and beam-azimuth of the incoming wavefronts for particular time intervals were calculated to analyze the observed glacial events. Then, the detected event signals were relocated and attributed to estimate the array parameters; slowness, azimuth, and back-azimuth.

The array response simulation parameters of the four selected events and their array response images for the GRSN seismic network were also estimated. FK-Array response to four Greenland glacial earthquakes concludes that the transfer function of GRSN array depends on the slowness of the glacial seismic phases and is a function of the wavenumber k (or frequency f) of the observed glacial signals, and of array geometry. The GRSN array geometry defines the resolution of the array for small wave-

numbers and the azimuth dependence. Several side lobes of the transfer function are the result of the larger distances between the single array sites.

Finally, this paper summarized the processing steps of the array processing technique used with array parameters computed from the SHM for detecting the events and associated seismic signals of the detected events from regional seismic events using array installation data from the GRSN array. This study also has complementary implications for the previously published, similar research including the same data set and GRSN array. The one of these is that the glacial seismicity associated with rapidly moving outlet glaciers in Greenland is a distinct long-period earthquake phenomenon, revealing a new category of earthquake source models in Polar Regions which are surprisingly aseismic. Considering the detected glacial events in this study, the array parameters using the array processing technique can be used to constrain the long-period glacio-mechanical and/or -tectonic processes active in Greenland and also Antarctica. This brings a new investigation of Greenland glacial seismicity updated to 2008.

Acknowledgements

This work was supported by Yuzuncu Yıl University, Department of Geophysical Engineering (Van, Turkey) and the University of Oulu, Sodankylä Geophysical Observatory (SGO), Laboratory of Applied Seismology (Oulu, Finland) with a post-doctoral research grant and training agreement contract issued to Yuzuncu Yıl and Oulu Universities. Thanks go to staff members of the University of Oulu and SGO. Their valuable suggestions to Seismic Handler experience in data analysis were taken into account. The author offers his greatest appreciation to the post-doctoral supervisor, Prof. Dr. Elena Kozlovskaya, Dr. Riitta Hurskainen who contributed to the sensitivity analyses in installing data package associated with array station coordinates and also processing the various sections of the waveforms (e.g., waveform correlation) and the Director of SGO, Prof. Dr. Esa Turunen. The author is also very grateful to Editors (Dr. Kimmo Kahma and Dr. Pekka Heikkinen) and two anonymous reviewers (Dr. Heidi Soosalu) for their careful reviews which considerably constructed the current study and helped to significantly improve the original draft.

References

- Bormann, P. (Ed.) 2012. New Manual of Seismological Observatory Practice (NMSOP-2), IASPEI, GFZ German Research Centre for Geosciences, Potsdam; <http://nmsop.gfz-potsdam.de>; doi: 10.2312/GFZ.NMSOP-2.
- Capon, J., 1969. Investigation of long-period noise at the large aperture seismic array. *J. Geophys. Res.*, **74**, 3182–3194.
- Ekström, G. 2006. Global detection and location of seismic sources by using surface waves. *Bulletin of the Seismological Society of America* **96**, 1201–1212.
- Ekström, G., M. Nettles and G.A. Abers, 2003. Glacial earthquakes. *Science* **302**, 622–624.

- Ekström, G., M. Nettles and V.C. Tsai, 2006. Seasonality and increasing frequency of Greenland glacial earthquakes. *Science* **311**, 1756–1758.
- Harjes, H.-P. and M. Henger, 1973. Array-Seismologie. *Z. Geophysik* **39**, 865–905 (in German).
- Haubrich, R.A., 1968. Array design. *Bull. Seism. Soc. Am.* **58**, 977–991.
- Kawakatsu, H., 1989, Centroid single force inversion of seismic waves generated by landslides. *Journal of Geophysical Research* **94**, 12363–12374.
- Korn, M., 2002 (Ed.). Ten years of German Regional Seismic Network (GRSN): Report 25 of the Senate Commission for Geosciences. Deutsche Forschungsgemeinschaft, Wiley-VCH Verlag, Weinheim, 2002.
- Moon, T and I. Joughin, 2008. Changes in ice front position on Greenland's outlet glaciers from 1992 to 2007. *J. Geophys. Res.* **113**, F02022.
- Nettles, M. and G. Ekström, 2010. Glacial earthquakes in Greenland and Antarctica. *Annual Review of Earth and Planetary Sciences* **38**(1), 467–491. doi: 10.1146/annurev-earth-040809-152414.
- Rost, S., and C. Thomas, 2003. Array seismology: Methods and applications. *Rev. Geophys.*, **40**(3), 1008. doi: 10.1029/2000RG000100.
- Schweitzer, J., J. Fyen, S. Mykkeltveit and T. Kvaerna, 2009. Seismic arrays, in: Bormann P. (Ed.). 2009, New Manual of Seismological Observatory Practice (NMSOP). Deutsches GeoForschungsZentrum, Potsdam, pp. 1–52. doi: 10.2312/GFZ.NMSOP_r1_ch9.
- Stammler, K., 1992, SeismicHandler - Programmable multichannel data handler for interactive and automatic processing of seismological analysis. *Computers & Geosciences* **19**, 135–140.
- Token, M., 2018. The Array Analyzing of the High Quality Glacial Seismic Events Active in Greenland Using Long-Period Surface (Rayleigh) Wave Detection by the German Regional Seismic Network. *Hittite Journal of Science and Engineering* **5**(2), 165–173, ISSN: 2148-4171; doi: 10.17350/HJSE19030000091.
- Trnkoczy, A., J. Havskov and L. Ottemöller, 2009. Seismic networks, in: Bormann P. (Ed.). New Manual of Seismological Observatory Practice (NMSOP). Deutsches GeoForschungsZentrum, Potsdam, pp. 1–60. doi: 10.2312/GFZ.NMSOP_r1_ch8.
- Tsai, V.C. and G. Ekström, 2007. Analysis of glacial earthquakes. *J. Geophys. Res* **112**, F03S22.